General Disclaimer

One or more of the Following Statements may affect this Document

- This document has been reproduced from the best copy furnished by the organizational source. It is being released in the interest of making available as much information as possible.

- This document may contain data, which exceeds the sheet parameters. It was furnished in this condition by the organizational source and is the best copy available.

- This document may contain tone-on-tone or color graphs, charts and/or pictures, which have been reproduced in black and white.

- This document is paginated as submitted by the original source.

- Portions of this document are not fully legible due to the historical nature of some of the material. However, it is the best reproduction available from the original submission.

NASA Technical Memorandum 78542

A Group-Velocity Criterion for Breakdown of Vortex Flow — An Application to Measured Inlet Profiles

Chon-Yin Tsai and Sheila E. Widnall

July 1979

National Aeronautics and
Space Administration

NASA Technical Memorandum 78542

A Group-Velocity Criterion for Breakdown of Vortex Flow — An Application to Measured Inlet Profiles

Chon-Yin Tsai, Ames Research Center, Moffett Field, California
Sheila E. Widnall, Massachusetts Institute of Technology, Cambridge, Massachusetts

NASA
National Aeronautics and
Space Administration

Ames Research Center
Moffett Field, California 94035

NOMENCLATURE

A	swirl parameter used in reference 1
C_g	group velocity of wave propagation in axial direction, $\frac{-d\omega}{dk}$
C_p	phase velocity of wave propagation in axial direction, $\frac{-\omega}{k}$
c	geometry parameter of the shape of the duct
k	axial wave number
n	azimuthal wave number
Q	a parameter defined by $\frac{\beta\sqrt{\alpha}}{\delta_1}$
q	a parameter defined by αr_i^2
$R(z)$	the geometry function of the shape of the duct
R_i	the radius at the inlet of the duct
Re	Reynolds number, defined by $\frac{2\bar{W}R_i}{\nu}$
r^*	the radial coordinate normalized by $R(z)$
(r,θ,z)	cylindrical coordinates sitting at the center of the inlet of a divergent duct
r_i	the radial coordinate at the inlet of the duct
(U,V,W)	velocities of basic flow field; U in radial direction, W in axial direction
V_w	swirl velocity along the wall of the duct
$\bar{W}$	average axial velocity from volume flow rate
W_o	axial velocity along the axis of the duct
W_w	axial velocity along the wall of the duct
$(\alpha,\beta,\delta_o,\delta_1)$	parameters of the best fit to the experimental data
Γ	circulation function
ζ_b	a parameter used in reference 1, $\frac{Re^{1/2}}{R_i}$
ν	kinematic viscosity of water

ψ stream function of the basic flow field

Ω swirl number, defined by $\frac{V_w}{W}$

ω frequency of the disturbances

A GROUP-VELOCITY CRITERION FOR BREAKDOWN OF VORTEX FLOW — AN APPLICATION TO MEASURED INLET PROFILES

Chon-Yin Tsai* and Sheila E. Widnall†

Ames Research Center

SUMMARY

A group-velocity criterion for vortex breakdown implied by Landahl's general wave trapping theory is applied to vortex flows exhibiting breakdown in a slightly divergent duct. The slowly varying vortex flow field downstream of the entrance and upstream of the breakdown region is obtained numerically by using the inviscid quasi-cylindrical approximation. In these calculations, the Faler and Lebovich's experimental data were used as the starting conditions at the entrance of the duct. The group velocity of wave propagation for the axisymmetric mode ($n = 0$) and the asymmetric modes ($n = \pm 1$ and $n = \pm 2$) are calculated for the entrance conditions. For the theoretically predicted slowly varying flow field downstream of the entrance, the wave characteristics of the $n = 0$ and $n = \pm 1$ modes are presented. It is found that the flows which subsequently undergo vortex breakdown are all predicted to be supercritical and stable to infinitesimal inviscid disturbances, including the axially symmetric as well as the nonsymmetric perturbations.

INTRODUCTION

Vortex breakdown is a natural characteristic of vortex motions in which swirl and axial flow are combined. The breakdown of the flow is usually identified by the formation of an internal stagnation point on the vortex axis, followed by reversed flow in a region of limited axial extent (ref. 2). Sarpkaya (ref. 3) and Faler and Lebovich (ref. 4) have classified several types of vortex breakdown based on their experiments and on flow visualizations in a slightly divergent duct. Their experimental results show that the type and location of the breakdown are governed by the ratio of the azimuthal to axial velocity components. They subsequently measured the detailed velocity of vortex flow field which exhibited breakdown in the same divergent duct by using laser Doppler anemometry (refs. 4, 5).

In the present study, the wave trapping analysis is applied to the experimental data measured by Faler and Lebovich (ref. 4) at the entrance of the duct and to the theoretically predicted velocity profiles downstream of the

*National Research Council Research Associate, Ames Research Center. Current Address: Boeing Commercial Airplane Company, Seattle, Washington.

†Professor in Department of Aeronautics and Astronautics, Massachusetts Institute of Technology, Cambridge, Mass.

entrance. The development of the slowly varying steady vortex flow in the duct is obtained by using the experimentally measured data as the input condition at the inlet of a divergent duct. The duct flow is then calculated by means of an inviscid quasi-cylindrical approximation. The linear-wave-propagation analysis is then applied to this base flow at each axial station. The dispersion relation is calculated numerically and from this the group velocity is obtained. Tsai and Widnall (ref. 6) also applied the linear-wave-propagation analysis to real vortex flows which were measured at several axial stations both upstream and downstream of the breakdown region obtained by Garg (ref. 5).

The authors gratefully acknowledge the valuable assistance and encouragement of Dr. Vernon J. Rossow.

ANALYSIS OF THE BASE FLOW FIELD

The flow apparatus used in the experiments is described in detail by Faler (ref. 7). The test section is a slowly divergent duct which consists of a linear change in the internal diameter from 3.81 cm to 5.08 cm over a length of 25.4 cm. The test apparatus permitted two parameters, Reynolds number ($Re = 2\bar{W}R_i/\nu$ where $\bar{W}$ is the average axial velocity from volume rate and R_i is the radius at the inlet of the test section) and swirl number ($\Omega = V_w/\bar{W}$ where V_w is the swirl velocity at the wall), to be systematically varied in the experiments. For a given set of parameters (Re, Ω), Faler and Lebovich (ref. 4) used flow visualization studies to reveal six distinct types of vortex breakdown. The types of flow disturbance observed and the mean axial location of the disturbance are summarized in figure 1. Two forms predominate, one called "near-axisymmetric" (sometimes "axisymmetric," or "bubble-like," or type 0) and the other called "spiral" (type 2). A series of measurements of the swirl (V) and the axial (W) velocity components were taken at a station located two-thirds of a tube radius upstream of the start of the diverging test section for various combinations of Reynolds numbers and swirl numbers. The resulting measured velocity components were represented approximately by a least squares fit of the data to the profiles.

$$V(r) = \frac{\beta}{r}\left(1 - e^{-\alpha r^2}\right) \tag{1}$$

$$W(r) = \delta_o + \delta_1 e^{-\alpha r^2} \tag{2}$$

where r is the radial location normalized with respect to the radius R_i. The parameters α, β, δ_o, and δ_1 were obtained by Garg (ref. 5) and are tabulated in table 1. (The wave-propagation analysis is applied to the base flow with slightly different value of these parameters. This set of slightly different values, written in parenthesis in table 1, was provided by S. Lebovich earlier than Garg's (ref. 5) publication.)

The development of a vortex flow in a slightly divergent duct, without any outside disturbances, can be obtained by means of an inviscid quasi-cylindrical approximation. With the input functions, equations (1) and (2), at the inlet of the duct, the upstream conditions are given by

$$\psi(r_i,\ z = 0) = \frac{\delta_o}{2} r_i^2 + \frac{\delta_1}{2\alpha}\left(1 - e^{-\alpha r_i^2}\right) \tag{3}$$

$$\Gamma(\psi) = \beta\left(1 - e^{-\alpha r_i^2}\right) \tag{4}$$

where r_i and z are the radial and axial coordinates from the center of the inlet of the divergent duct; ψ and Γ are the stream function and the circulation function, respectively.

For a slightly divergent duct, a quasi-cylindrical approximation can be used to obtain the vortex flow field. The governing equation for the stream function ψ can be written as follows (ref. 8):

$$\frac{d^2\psi}{dr^2} - \frac{1}{r}\frac{d\psi}{dr} = r^2\left(\frac{\Gamma}{r_i}\frac{d\Gamma}{d\psi} + W\frac{dW}{d\psi}\right) - \Gamma\frac{d\Gamma}{d\psi} \tag{5}$$

Substitution of the upstream conditions (3) and (4) into the right-hand side of equation (5) yields

$$\frac{d^2\psi}{dr^{*2}} - \frac{1}{r^*}\frac{d\psi}{dr^*} = r^{*2}R^4(z)\left[-2\alpha\delta_1 e^{-q} + \frac{2\beta^2\alpha^2(1 - e^{-q})e^{-q}}{\left(\delta_o + \delta_1 e^{-q}\right)q}\right]$$

$$- R^2(z)\,\frac{2\beta^2\alpha(1 - e^{-q})e^{-q}}{\delta_o + \delta_1 e^{-q}} \tag{6}$$

where q is calculated by inverting the equation

$$\psi(q;z = 0) = \frac{\delta_o}{2\alpha} q + \frac{\delta_1}{2\alpha}\left(1 - e^{-q}\right) \tag{7}$$

and

$$R(z) = 1 + z \tan 1.43^\circ = 1 + 0.025z$$

$$q = \alpha r_i^2$$

$$r^* = r/R(z)$$

with z normalized by R_i. The boundary conditions are

$$\psi(r^* = 0, z) = 0 \tag{8}$$

$$\psi(r^* = 1,z) = \frac{\delta_o}{2} + \frac{\delta_1}{2\alpha}\,(1 - e^{-\alpha}) \tag{9}$$

Since equations (6) and (7) are nonlinear, the solution has to be obtained numerically. The procedure is as follows: at each axial station z, we use

$$\psi(r^* = 10^{-5}) = \frac{\delta_o}{2}\,r^{*2} + \frac{GUESS}{2\alpha} \cdot \left(1 - e^{-\alpha r^{*2}}\right)$$

$$\frac{d\psi}{dr^*}\,(r^* = 10^{-5}) = \delta_o r^* + GUESS \cdot r^* e^{-\alpha r^{*2}}$$

as the initial condition to start the integration in the radial direction. The value of "GUESS" used in the foregoing equation is the solution obtained at the previous axial station. The correct numerical result is then determined by an iteration process in order to satisfy the boundary condition at $r^* = 1$. Since we cannot express q in terms of ψ explicitly from equation (7), we have to calculate q numerically from ψ at each step of the integration in the radial direction in order to continue the integration to the next step in the radial direction. At each axial station, the numerical solution is checked by two conditions: (1) the total head function $H(\psi)$ must be conserved along the stream line; and (2) the difference in the axial gradient of the axial velocity along the wall and along the axis is given by

$$\frac{dW_o^{\,2}}{dz} - \frac{dW_w^{\,2}}{dz} = 2\int_0^R \frac{1}{r^3}\,\frac{\partial \Gamma^2}{\partial z}\,dr$$

where $W_o = W(r = 0,z)$ and $W_w = W(r = R,z)$. The above numerical solution is restricted to positive ψ; that is, a reverse flow region is not allowed.

The computer program for the inviscid quasi-cylindrical approximation to a vortex flow was first applied to the case of constant vorticity and uniform axial velocity at the inlet of a divergent duct. The comparison between the numerical results and the well-known analytical solution was good. This computer program was then applied to input velocity profiles of the form $V = \beta(1 - e^{-20r^2})/r$ and $W = 1.0$ in a duct of the shape $R(z) = (1 + cz)^{-1/2}$. The parameters β in the foregoing equation are 0.25, 0.275 and 0.30. These cases are equivalent to those of Hall (ref. 1) with $A = 10.0$, 11.0, 12.0, and $\zeta_b = 40.0$, where A is the swirl parameter and $\zeta_b = Re^{1/2}R_i$. The numerical results obtained from the present computer program are shown in figures 2-4. The results obtained by Hall's numerical method including viscous effects are reproduced in figures 5-7. It can be seen that two solutions show the same characteristics qualitatively, although not quantitatively, because the Reynolds number used in Hall's case (Re = 1600) was too small to compare with the inviscid case. From the comparison of the inviscid quasi-cylindrical calculations with those of Hall, we conclude that although the qualitative behavior of a slightly viscous flow is predicted by the inviscid theory, the quantitative behavior is not. The effects of viscosity become

more pronounced as the duct becomes more gradual and as the swirl velocity increases. In general, the position of the failure of the quasi-cylindrical calculation in a viscous supercritical flow will occur upstream of that for inviscid flow.

We then apply the present computer program to the various velocity profiles listed in table 1. Figure 8 shows the variation of the axial velocity along the axis for different initial values of the swirl parameters of $V = \beta(1 - e^{-15.69r^2})/r$ and $W = 1 + 1.137\ e^{-15.69r^2}$ (case 4 with variable β) within the fixed shape of the duct $R(z) = 1 + 0.025z$. It can be seen that the convergence of the inviscid quasi-cylindrical approximation solution is sensitive to the swirl parameter β. For $\beta = 0.507$, which is case (4) in experiments (table 1), the inviscid quasi-cylindrical approximation fails around $z = 16.45$. The theoretically calculated profiles of the axial velocity and the swirl velocity at each axial stations are shown in figure 9. The flow visualization studies for the case (4), from figure 1, reveal that the spiral form breakdown was dominant at about $z = 5.4$ and the axisymmetric form of breakdown either formed around $z = 3.9$ and did or did not persist. Figures 10-12 show another calculation for cases (1), (2) and (3) (table 1). It can be seen that, in these four cases, the experimentally observed breakdown occurs at an axial location upstream of the failure of the quasi-cylindrical approximation (table 2). (Only four locations of the failure of the inviscid quasi-cylindrical approximation are presented in table 2.)

The present computer program is also applied to the Garg's (ref. 5) data which have been measured at higher Reynolds number than those of Faler and Lebovich, and at several downstream stations. For the flow exhibiting spiral form of breakdown, Garg's data have been given at one more station ahead of the breakdown region. Therefore, the comparison between the best-fit curve of experimentally measured data and the inviscid quasi-cylindrical approximate solution can be made. However, it can be seen from figures 13-15, that the comparison is not good. If we check the volume flow rate and the circulation at two axial stations ahead of the breakdown region, it was found that the volume flow rate of best-fits for the measured data increases 14.7%, 10.8%, and 5.9%; the circulation decreases 13.9%, 10.1%, and 12.5% at $Re = 11480$, $\Omega = 0.787$, $Re = 14100$, $\Omega = 0.741$ and $Re = 20660$, $\Omega = 0.682$, respectively. Since a discrepancy between the volume flow rate of the best fit to the experimentally measured data at the two axial stations decreases as Re increases, it shows that the viscous effect is important in the low Re cases. Therefore, the viscous effect in Faler and Lebovich's cases, which were measured at much lower Re than Garg's, is believed to be important in their experiment. We were unable, under the present program, to include viscous effects in our calculations; this clearly should be done in the future.

It is still of considerable interest to calculate the wave propagation characteristics of the inviscid quasi-cylindrical development of the inlet profiles measured by Faler and Lebovich (ref. 4), even if the discrepancy between the mean flow and inviscid calculations remains to be resolved.

WAVE CALCULATIONS AND DISCUSSION OF RESULTS

Landahl (ref. 9) developed a general theory for the wave mechanics of breakdown to determine under what conditions the steady or unsteady laminar flow will breakdown into high frequency oscillations. Bilanin (ref. 10) applied Landahl's theory to vortex flows and concluded that the breakdown criterion for steady vortex flow in a slowly divergent duct requires that the group velocity C_g of infinitesimal waves be zero. The vortex flow may then be classified as "supercritical" when the group velocity of the infinitesimal wave propagates in the downstream direction ($C_g > 0$), and "subcritical" if the wave can propagate in either direction. The dispersion relations, and hence the group velocities, are obtained here by solving the eigenvalue problem at each axial station as if the flow were locally parallel. The location at which the group velocity of the wave disturbance is zero is the place where wave trapping occurs and it has been proposed that the vortex flow would also breakdown there. Typically, only one type (axisymmetric or spiral) wave mode would be critical at any station in the flow.

Except for special case of uniform vorticity and axial flow, the dispersion relation of linear wave propagation on a parallel flow field $(0, V(r), W(r))$ bounded by a rigid cylindrical tube $0 \leq r \leq 1$ has to be obtained numerically. Waves were assumed to be of the form

$$\{u, v, w\} = \{\tilde{u}, \tilde{v}, \tilde{w}\}e^{i(\omega t+n\theta+kz^*)}$$

so that the phase velocity is given by

$$C_p = -\omega/k$$

and the group velocity by

$$C_g = -d\omega/dk$$

Note that z^* is a local axial coordinate that is distinct from z used in the last section. The governing equation for this flow can be found in Lessen, Singh and Paillet (ref. 11). Hultgren (ref. 12) presented a numerical method that uses Moulton's method for the stability calculation of rotating gas flows. By using this computer program, it was possible to search for the eigenvalues for different cases listed in table 1 and also for their downstream development of the flow fields.

We use δ_o as the velocity scale and $R(z)$ as the length scale for the wave calculations. The characteristics of wave propagation for modes $n = 0, \pm1, \pm2$ on the velocity fields measured at inlet (listed in table 1) have been investigated numerically. It was found that the vortex flows that exhibit various types of breakdown are supercritical to these five modes of disturbances. Since there are similarities in wave characteristics among these eight cases, only the results for the wave characteristics of the inlet flow for case (8) (exhibiting Type 4 breakdown) are presented in figures 16-20. It can be seen that the minimum value of the group velocity is the same order

of magnitude for modes $n = 0$ and $n = 1$. However, the group velocities of mode $n = -1$ and $n = \pm 2$ have larger values than both modes $n = 0$ and $n = 1$. This indicates that we can ignore the downstream development of the $n = -1$ and $n = \pm 2$ modes. More detailed calculations confirmed this statement.

The wave characteristics (C_g vs k) at each station in the downstream development of the flow are shown in figures 21-27 for cases (1-4) of tables 1 and 2. On these figures, the wave number k has been nondimensionalized by the local radius $R(z)$. For mode $n = 0$, it can be seen that the group velocity C_g crosses zero near the place where the inviscid quasi-cylindrical approximation fails. Since the inviscid quasi-cylindrical approximation is a long-wavelength limit for axisymmetric wave, the group-velocity criterion ($C_g = 0$) for axisymmetric type of breakdown corresponds to the failure of the quasi-cylindrical approximation. For modes $n = +1$, the group velocity does not cross zero at any axial station. Although the group-velocity criterion for vortex breakdown ($C_g = 0$) does not occur for modes $n = +1$, the magnitude of the group velocity decreases with increasing downstream distance. It may be that a "finite amplitude" wave would be able to stand in this region of the flow. A direct comparison cannot be made of the experimentally observed axial location where the breakdown occurs with the theoretically predicted location for wave trapping since the mean flow is not adequately predicted by the inviscid calculations.

CONCLUSIONS

Although the original intent of the study (to use the group-velocity criterion to predict breakdown for experimentally determined initial data and then comparing the experimentally and theoretically determined location of the vortex breakdown point) was not completely realized, some conclusions can be drawn:

1. All flows that exhibit vortex breakdown of the "axisymmetric" form or "spiral" form are supercritical upstream, in that the group velocities of mode $n = 0$ or $n = 1$ are directed downstream. The group velocity of mode $n = -1$ is directed downstream with a speed larger than that for the mode $n = 1$; therefore, in a linear wave-trapping theory of vortex breakdown mode $n = -1$ is not the mode responsible for the spiral form of breakdown. The phase velocity of modes $n = -1$ and $n = -2$ can be in either direction, depending on the wave number k. In fact, the numerical results show that the phase velocity is directed upstream in the long wave limit of mode $n = -1$.

2. The group velocity of $n = 0$ and $n = 1$ wave propagation on a supercritical flow in a divergent duct becomes smaller as the axial location moves downstream. This may imply that the waves do have a tendency to eventually be trapped; however, since it is likely that vortex breakdown is a nonlinear phenomenon, the linear wave-trapping theory cannot be applied to the region near breakdown although it is useful for characterizing the state of the flow. The computer program for the linear wave-propagation analysis is also limited to the application of parallel flow.

3. The parameters Q in table 1 are larger than 1.5 for eight experimental cases. Therefore, according to the numerical results of Lessen et al. (ref. 11), all flows that exhibit vortex breakdown are stable upstream of the breakdown position to all modes of disturbances. Our numerical calculations also indicated that all of these flows were stable upstream of breakdown.

4. Viscous effects on the downstream development of the mean flow should be included even at moderate Reynolds numbers.

REFERENCES

1. Hall, M. G.: A New Approach to Vortex Breakdown. Proc. Heat Transfer Fluid Mech. Inst., 1967, pp. 319-340.

2. Lebovich, S.: The Structure of Vortex Breakdown. Ann. Rev. Fluid Mech., vol. 10, 1978, p. 221.

3. Sarpkaya, T.: On Stationary and Travelling Vortex Breakdown. J. Fluid Mech., vol. 45, pt. 3, 1971, p. 545.

4. Faler, J. H.; and Leibovich, S.: Disrupted States of Vortex Flow and Vortex Breakdown. Phys. Fluids, vol. 20, no. 9, 1977.

5. Garg, A. K.: Oscillatory Behavior in Vortex Breakdown Flows: An Experimental Study Using a Laser Doppler Anemometer. M.S. thesis, Cornell University, Ithaca, N.Y., 1977.

6. Tsai, C. Y.; and Widnall, S. E.: An Examination of Group-Velocity Criterion for Breakdown of Vortex Flow. Submitted to Phys. Fluids.

7. Faler, J. H.: Some Experiments in Swirling Flows: Detailed Velocity Measurements of a Vortex Breakdown Using a Laser Doppler Anemometer. Ph.D thesis, Cornell University, Ithaca, N.Y., 1976.

8. Batchelor, G. K.: An Introduction to Fluid Dynamics, Cambridge University Press, 1967.

9. Landahl, M. T.: Wave Mechanics of Breakdown. J. Fluid Mech., vol. 56, pt. 4, 1972, p. 775.

10. Bilanin, A. J.: Wave Mechanics of Line Vortices. Ph.D thesis, Massachusetts Institute of Technology, Cambridge, Mass., 1973.

11. Lessen, M., Singh, P. J.; and Paillet, F.: The Stability of a Trailing Line Vortex. Pt. 1. Inviscid Theory. J. Fluid Mech., vol. 63, pt. 4, 1974, p. 753.

12. Hultgren, L.: Ph.D Thesis, Massachusetts Institute of Technology, Cambridge, Mass., 1978.

TABLE 1. - THE LEAST SQUARES BEST FIT OF THE EXPERIMENTAL DATA TO THE EQUATIONS (1) and (2)

Case	Re	Ω	Z cm	δ_0, cm/sec	δ_1, cm/sec	β, cm/sec	α	Q
1	6000	1.282	-1.3	13.870 (13.80)	18.903 (18.66)	7.013 (6.60)	19.493 (22.53)	1.711
2	6000	1.068	-1.3	14.220 (14.20)	13.587 (13.88)	5.832 (5.65)	19.311 (21.14)	1.886
3	6000	.727	-1.3	14.720 (14.70)	7.181 (7.09)	3.980 (4.10)	19.462 (18.05)	2.445
4	4540	1.282	-1.3	10.630 (10.55)	12.077 (12.00)	5.204 (5.35)	16.408 (15.69)	1.745
5	4540	1.068	-1.3	10.890 (10.90)	9.352 (9.33)	4.399 (4.44)	15.671 (15.63)	1.862
6	4540	.727	-1.3	11.290 (11.20)	4.946 (4.97)	3.080 (3.19)	15.689 (14.41)	2.467
7	3220	1.541	-1.3	7.210 (7.25)	8.685 (8.47)	4.179 (4.31)	13.524 (12.37)	1.770
8	3220	1.068	-1.3	7.670 (7.70)	4.646 (4.67)	3.017 (2.99)	12.117 (12.53)	2.260

Note: The numerical values in ( ) were provided by S. Lebovich earlier than Garg's (ref. 5) publication.

TABLE 2. - THE COMPARISON OF POSITION BETWEEN THE EXPERIMENTALLY OBSERVED VORTEX BREAKDOWN AND THE FAILURE OF INVISCID QUASI-CYLINDRICAL APPROXIMATION

Case	Re	Swirl number	Type of breakdown	Observed mean position of breakdown, cm	Position of the failure of inviscid quasi-cylindrical approximation, cm
1	6,000	1.282	Axisymmetric	3.33	29.5
2	6,000	1.068	Spiral	13.83	30.8
3	6,000	.727	Uncertain	Uncertain	35.2
4	4,540	1.282	Axisymmetric	7.87	31.4
			Spiral	10.67	
5	4,540	1.068	Spiral	17.87	
6	4,540	.727	Uncertain	Uncertain	
7	3,220	1.541	Axisymmetric	3.33	
8	3,220	1.068	Type 4	18.57	
Garg's Data (ref. 5)					
	20,660	0.819	Axisymmetric	4.6	
	20,660	.682	Spiral	15.2	
	14,100	.884	Axisymmetric	5.6	
	14,100	.741	Spiral	15.5	
	11,480	1.066	Axisymmetric	2.3	
	11,480	.787	Spiral	15.5	

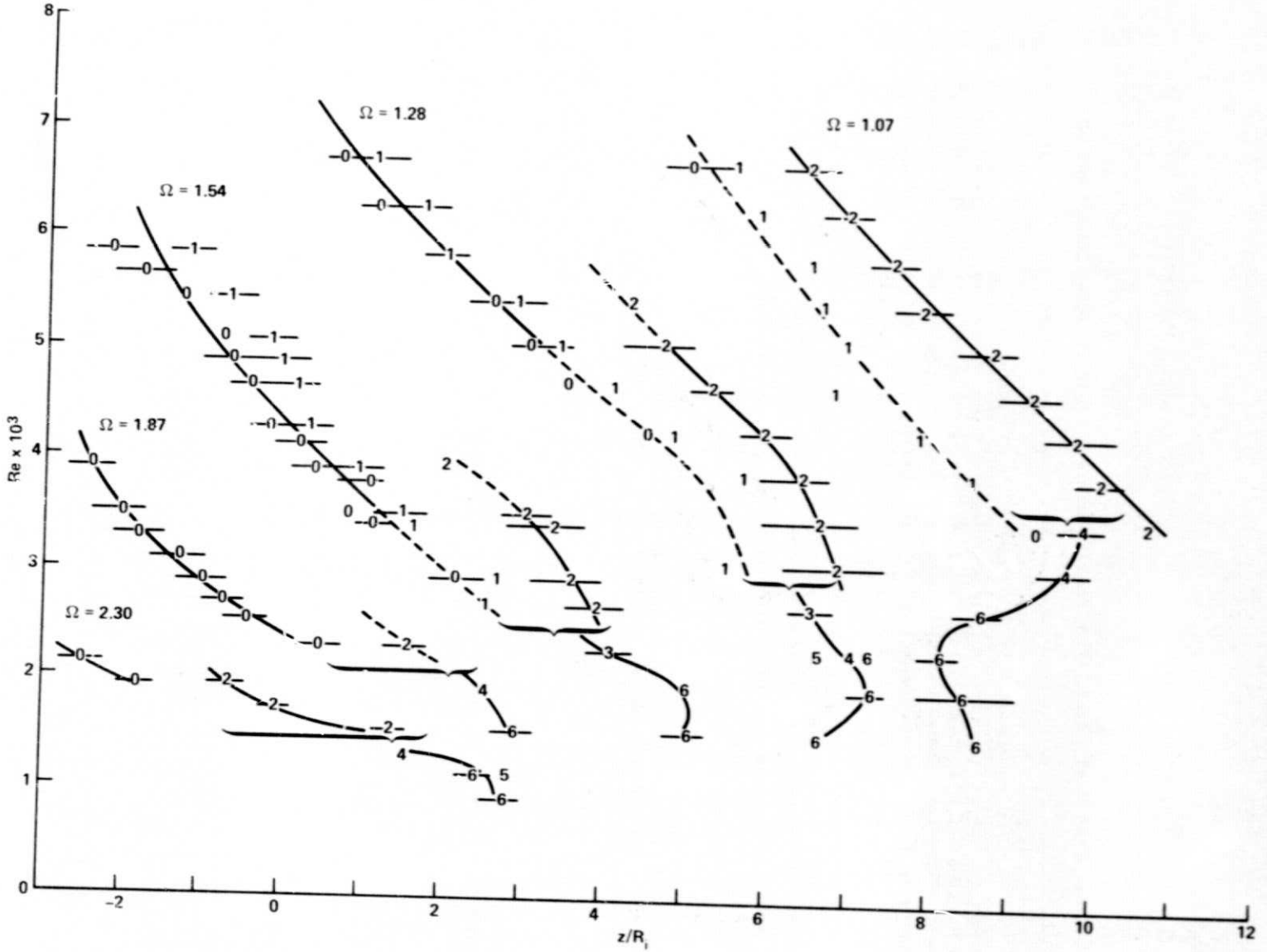

Figure 1.- The type of disturbance (0 - 6) and its mean axial location vs Reynolds number for five values of Ω (ref. 4).

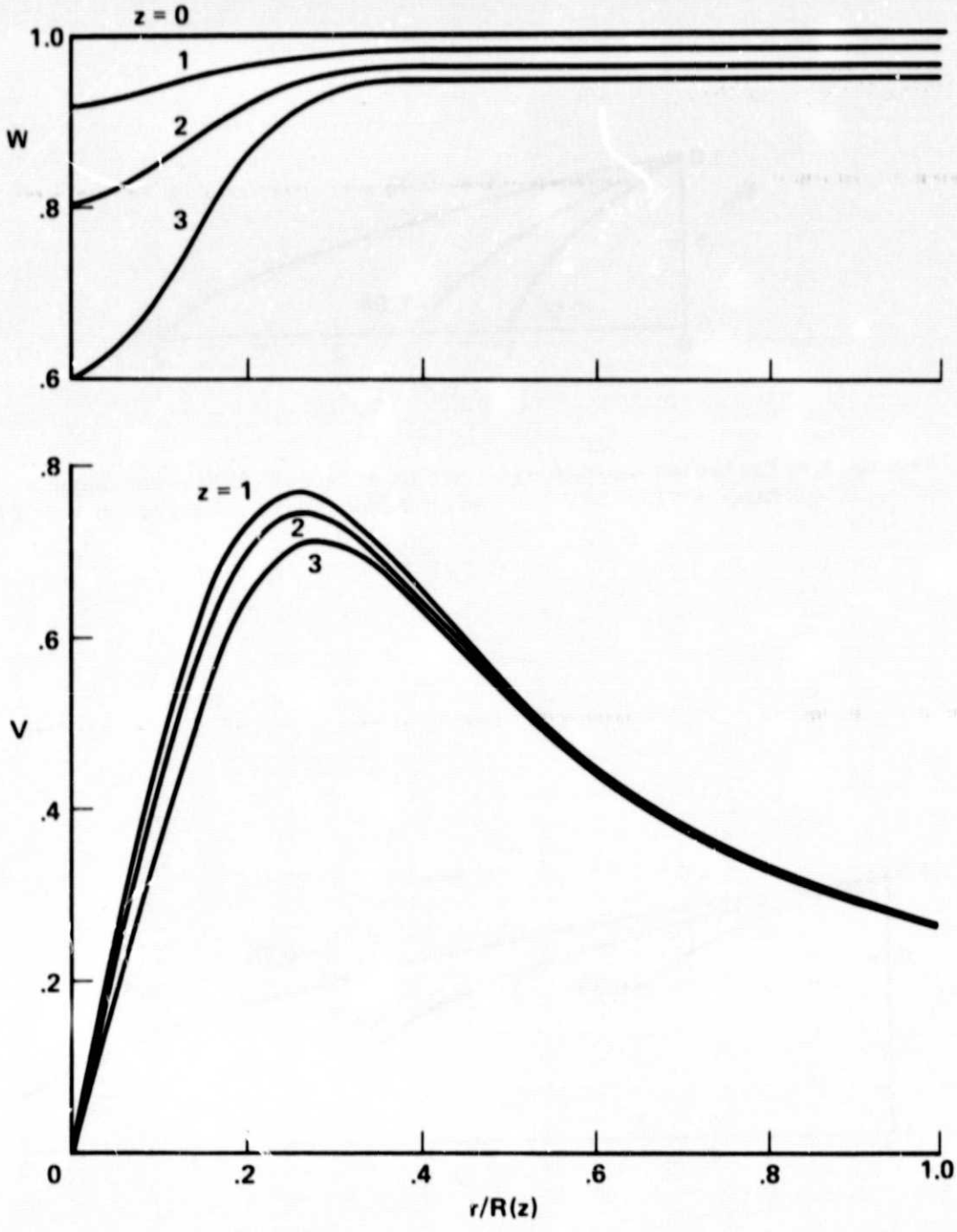

Figure 2.- Calculated profiles of axial (W) and swirl (V) velocity for initial velocity; $V = 0.275\ (1 - e^{-20r^2})/r$; $W = 1.0$ at the inlet of the duct with shape; $R(z) = (1 - 0.02z)^{-1/2}$.

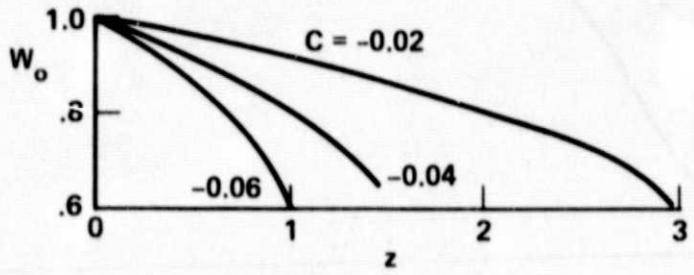

Figure 3.- Variation of velocity along axis for different shapes; $R(z) = (1 + Cz)^{-1/2}$ with fixed initial swirl $\beta = 0.275$.

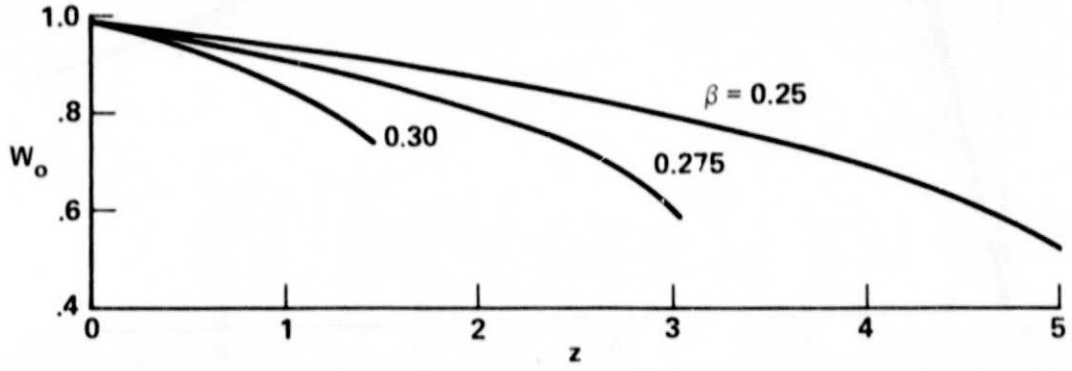

Figure 4.- Variation of velocity along axis for different initial swirls β with fixed shape; $R(z) = (1 - 0.02z)^{-1/2}$.

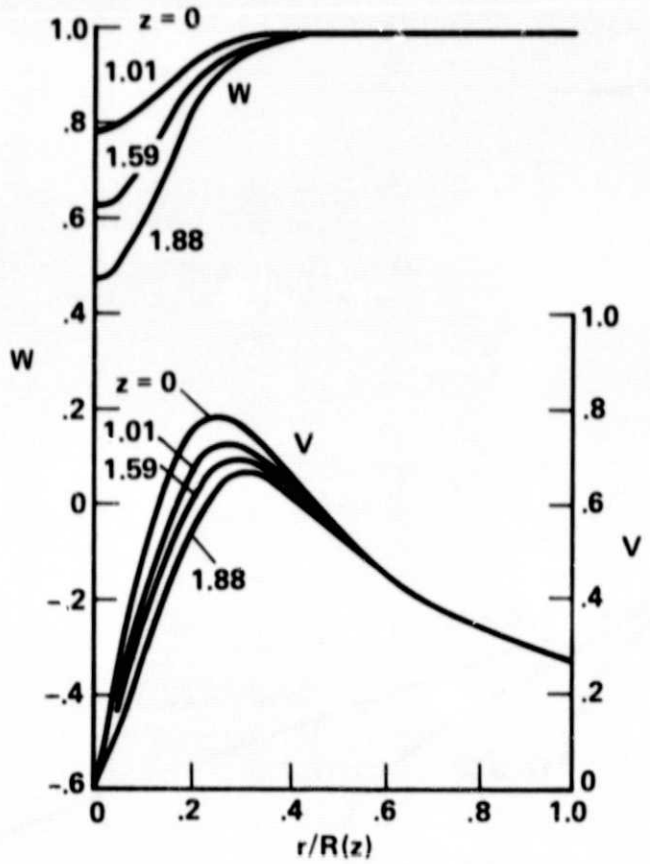

Figure 5.- Profiles of axial (W) and swirl (V) velocity for A = 11.0; C = -0.02 (ref. 1).

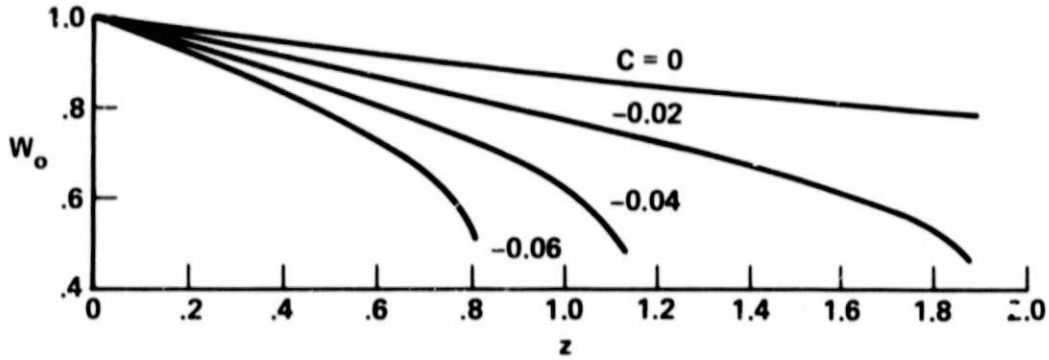

Figure 6.- Variation of velocity along axis for different shapes; $R(z) = (1 + Cz)^{-1/2}$, with fixed initial swirl; A = 11.0 (ref. 1).

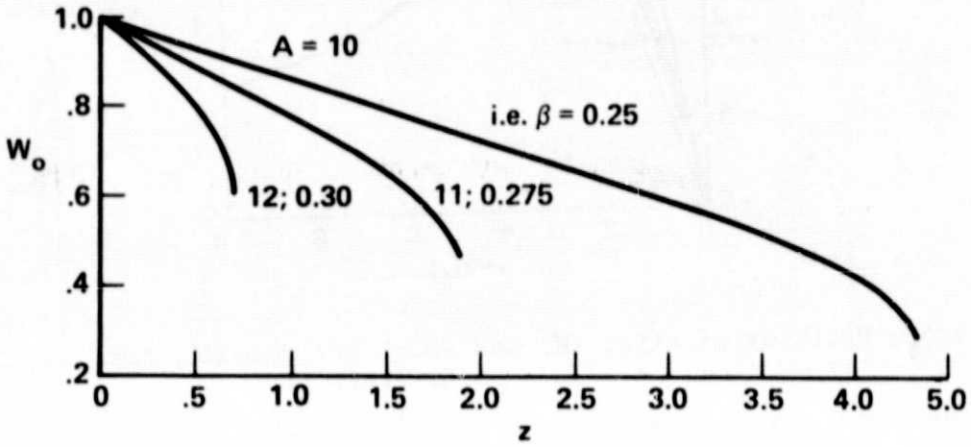

Figure 7.- Variation of velocity along axis for different initial swirls, with fixed shape; $R(z) = (1 - 0.02z)^{-1/2}$ (ref. 1).

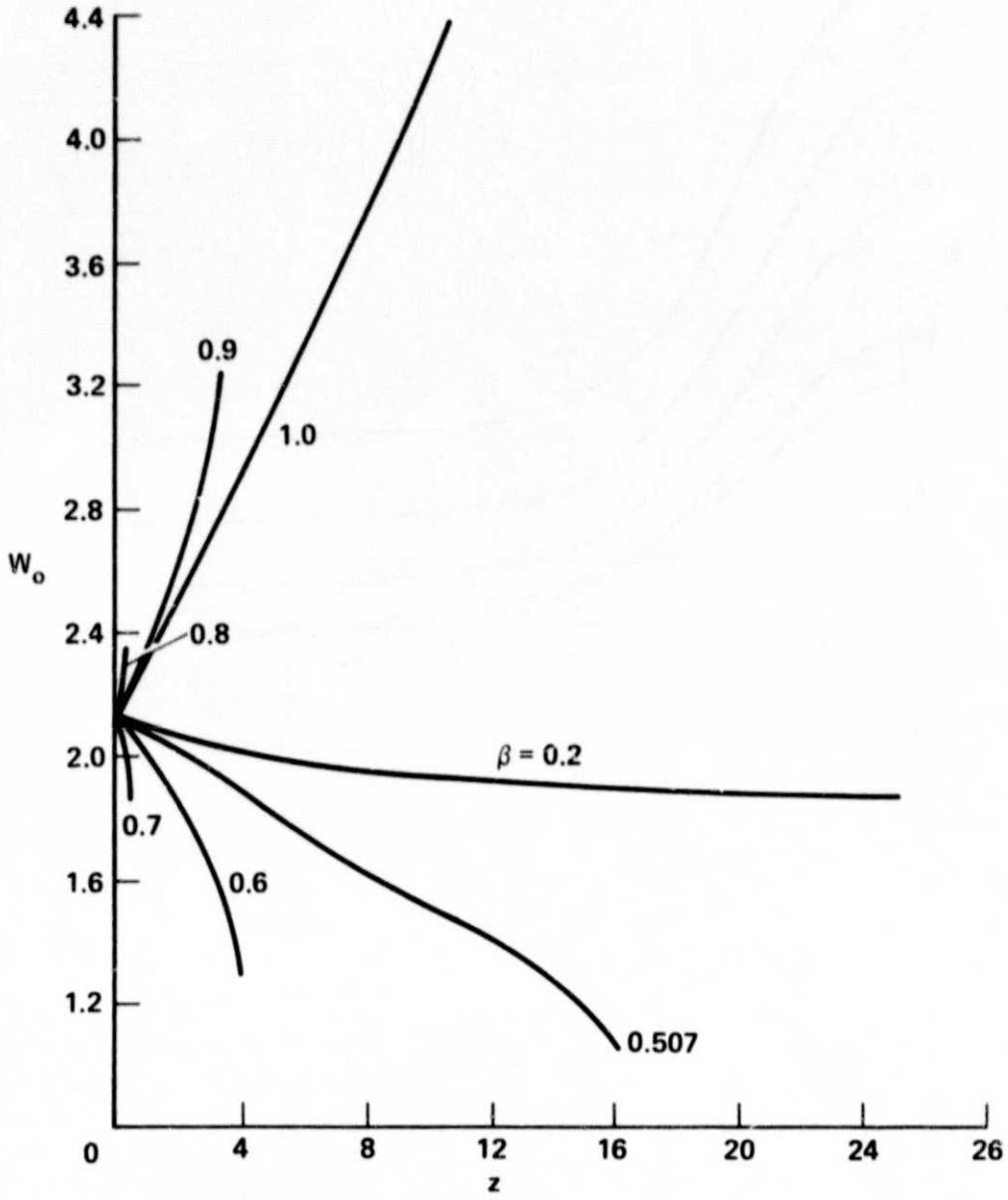

Figure 8.- Variation of velocity along axis for different initial swirls β of $V = \beta(1 - e^{-15.69r^2})/r$; $W = 1 + 1.137e^{-15.69r^2}$ in the duct with fixed shape; $R(z) = 1 + 0.025z$.

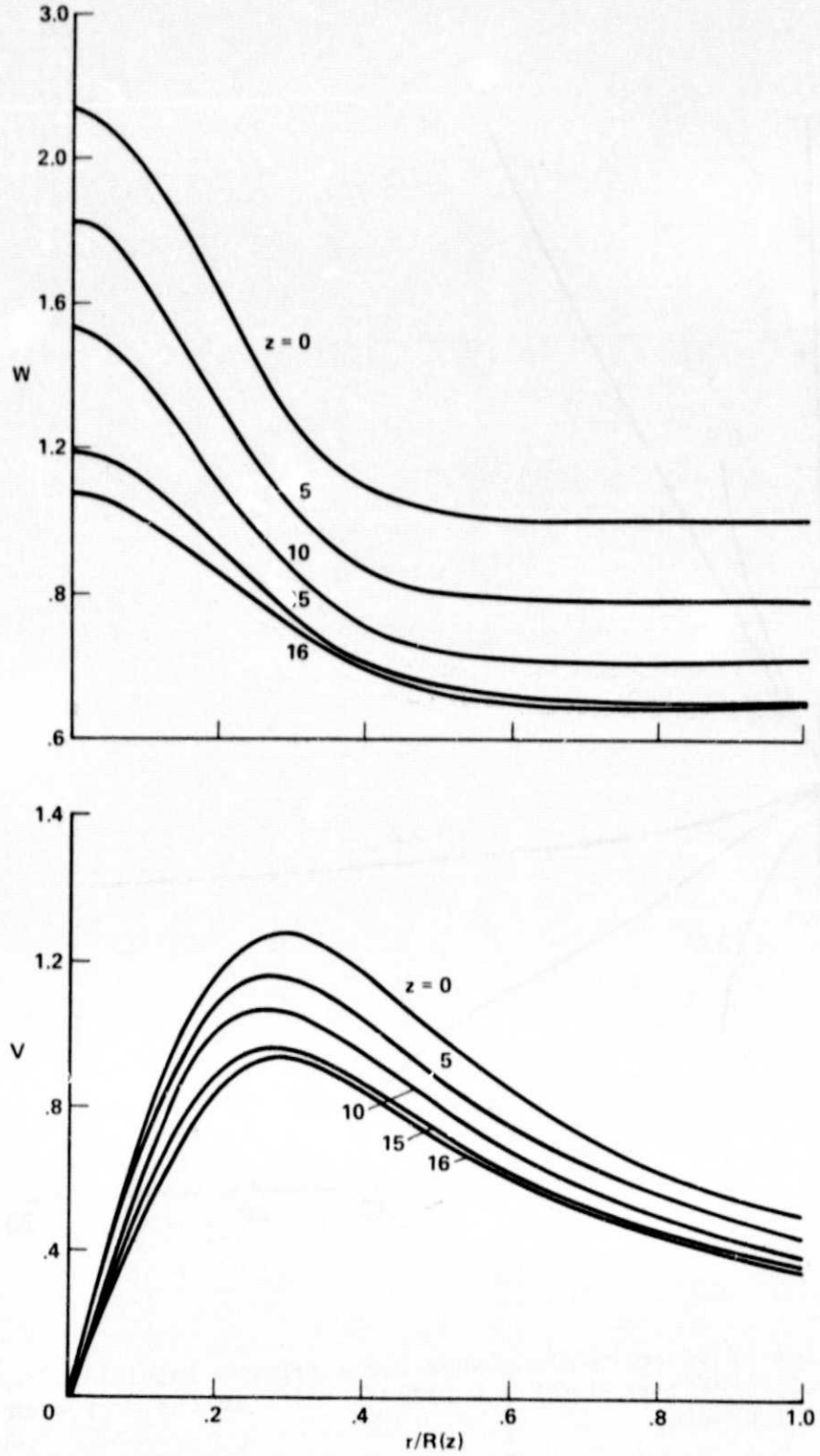

Figure 9.- Calculated profiles of axial (W) and swirl (V) velocity for case (4) in the duct with fixed shape; R(z) = 1 + 0.025z.

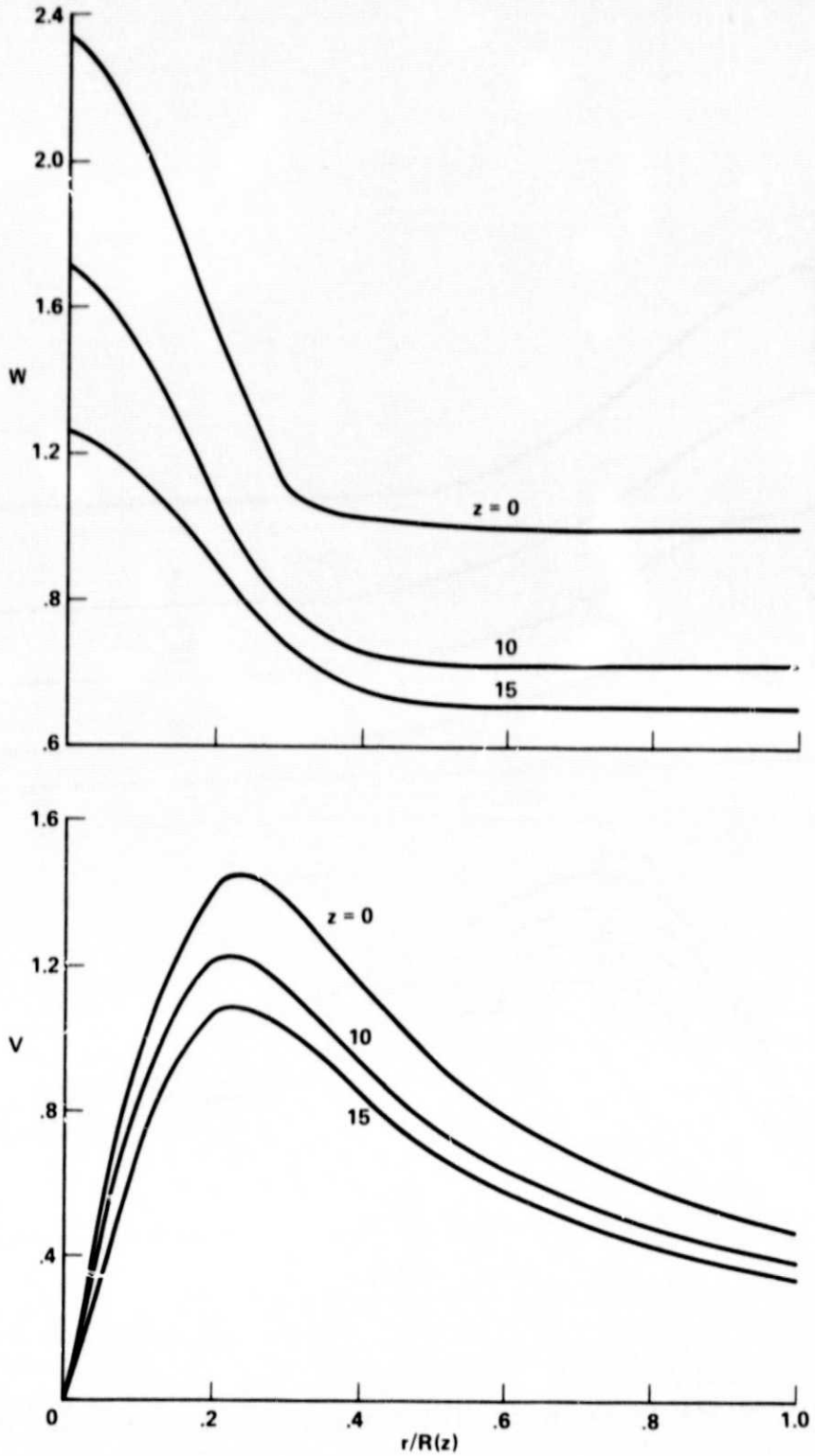

Figure 10.- Calculated profiles of axial (W) and swirl (V) velocity for case (1) in the duct with fixed shape; R(z) = 1 + 0.025z.

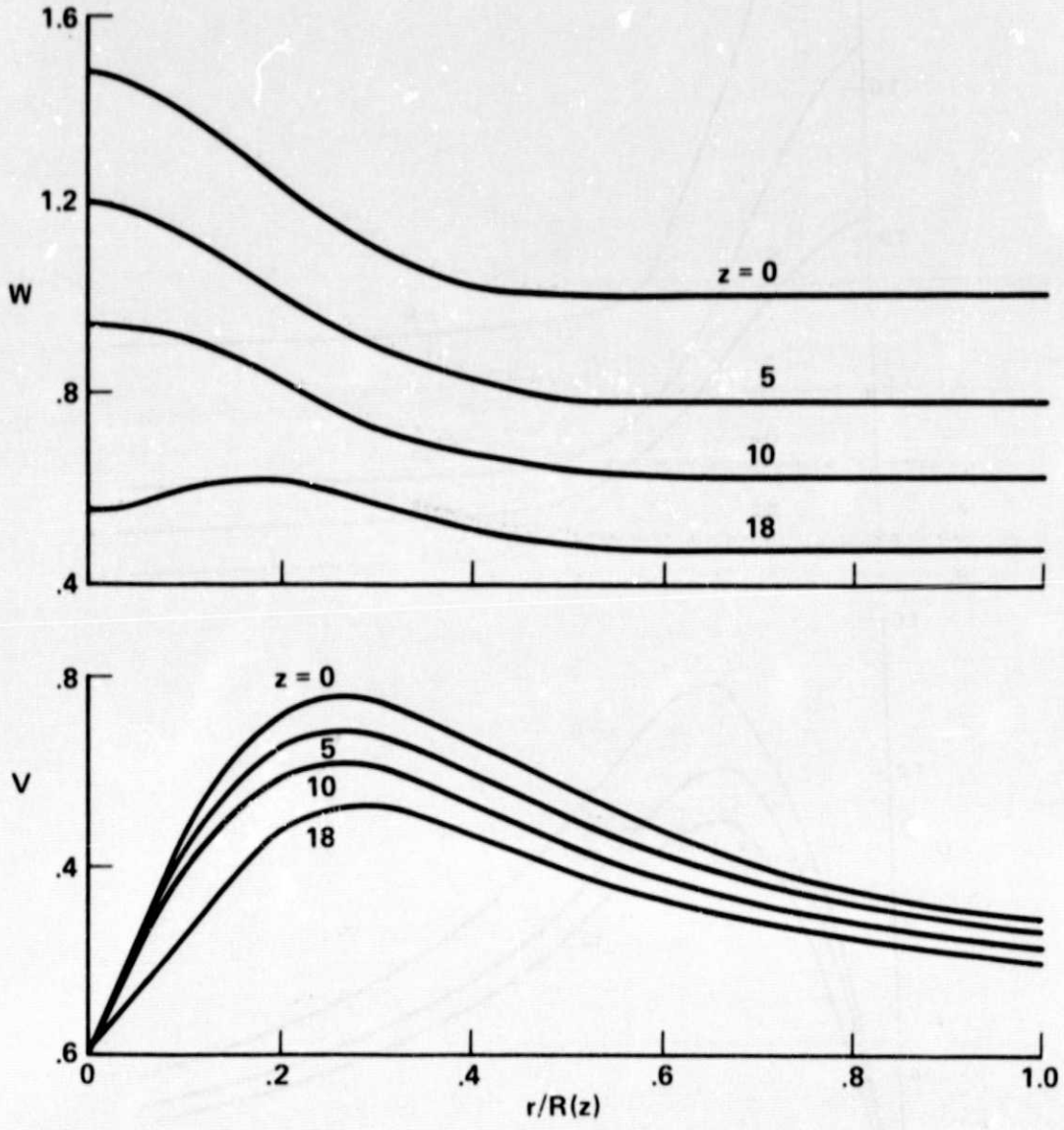

Figure 11.- Calculated profiles of axial (W) and swirl (V) velocity for case (2) in the duct with fixed shape; R(z) = 1 + 0.025z.

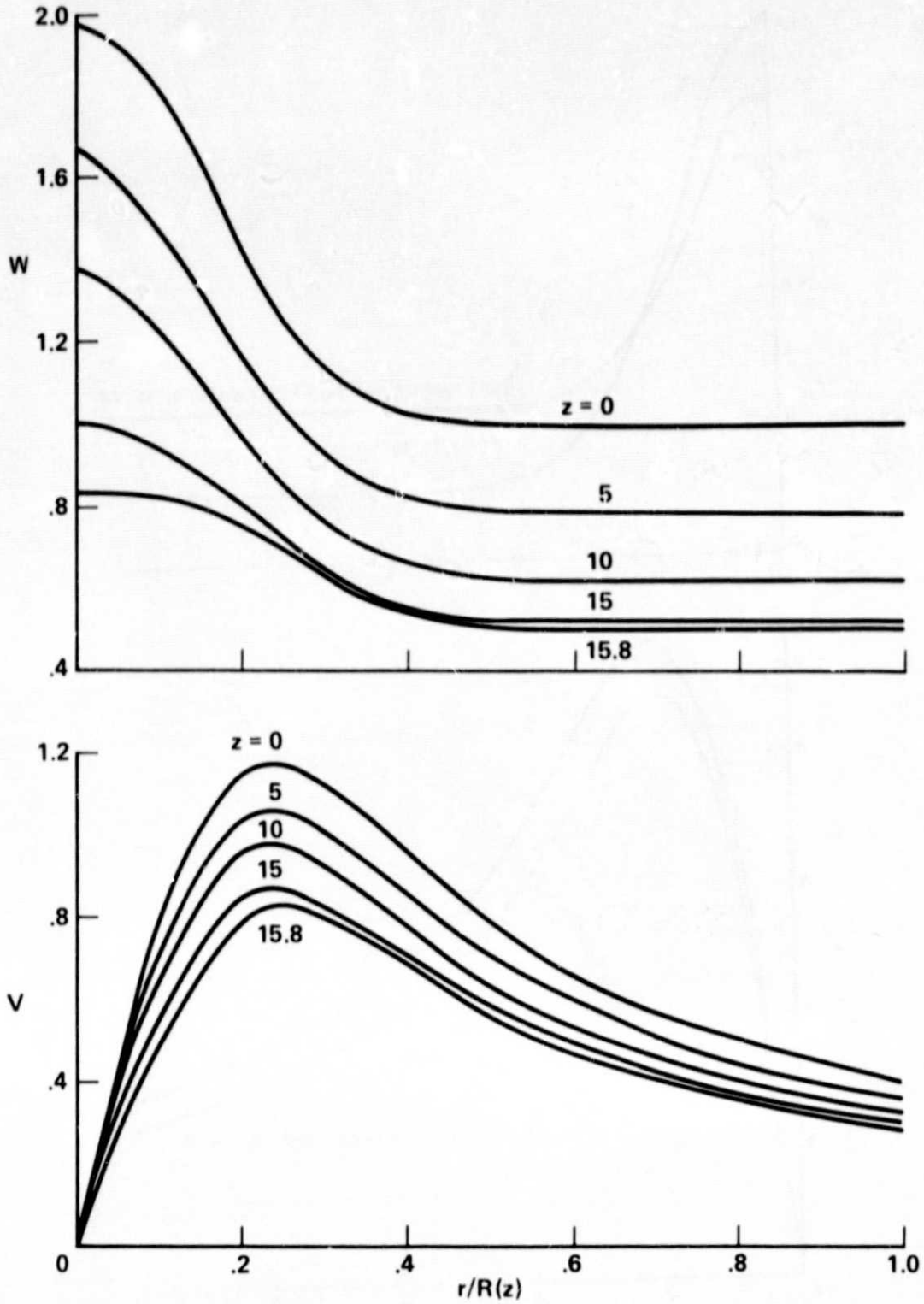

Figure 12.- Calculated profiles of axial (W) and swirl (V) velocity for case (3) in the duct with fixed shape; R(z) = 1 + 0.025z.

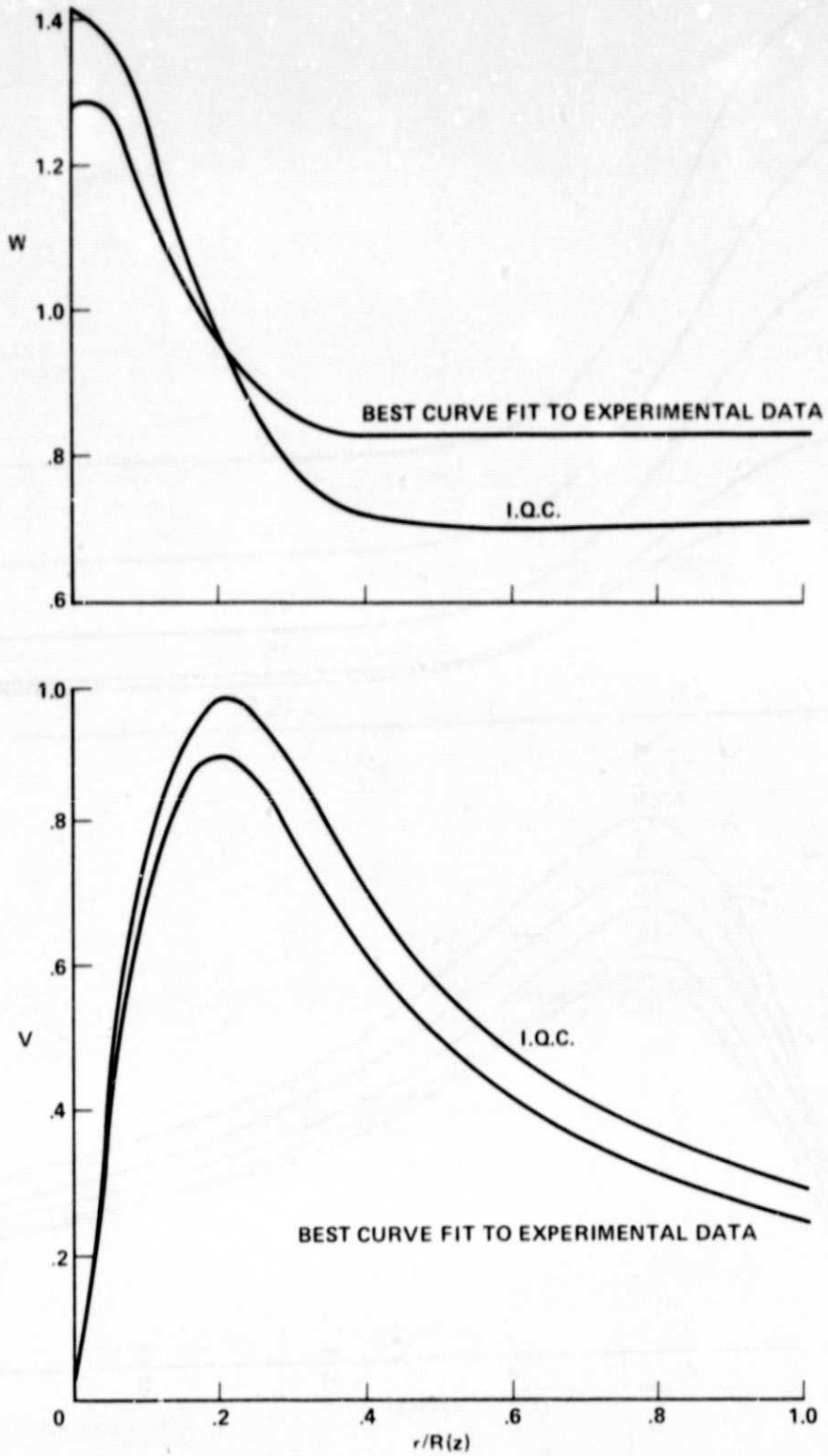

Figure 13.- Comparison of axial (W) and swirl (V) velocities between the best curve fit to experimental data and inviscid quasi-cylindrical solution (I.Q.C.) at axial stations; $z = 7.4$ for $Re = 11480$; $\Omega = 0.787$ at the inlet of the duct with shape; $(R(z) = 1 + 0.025z$.

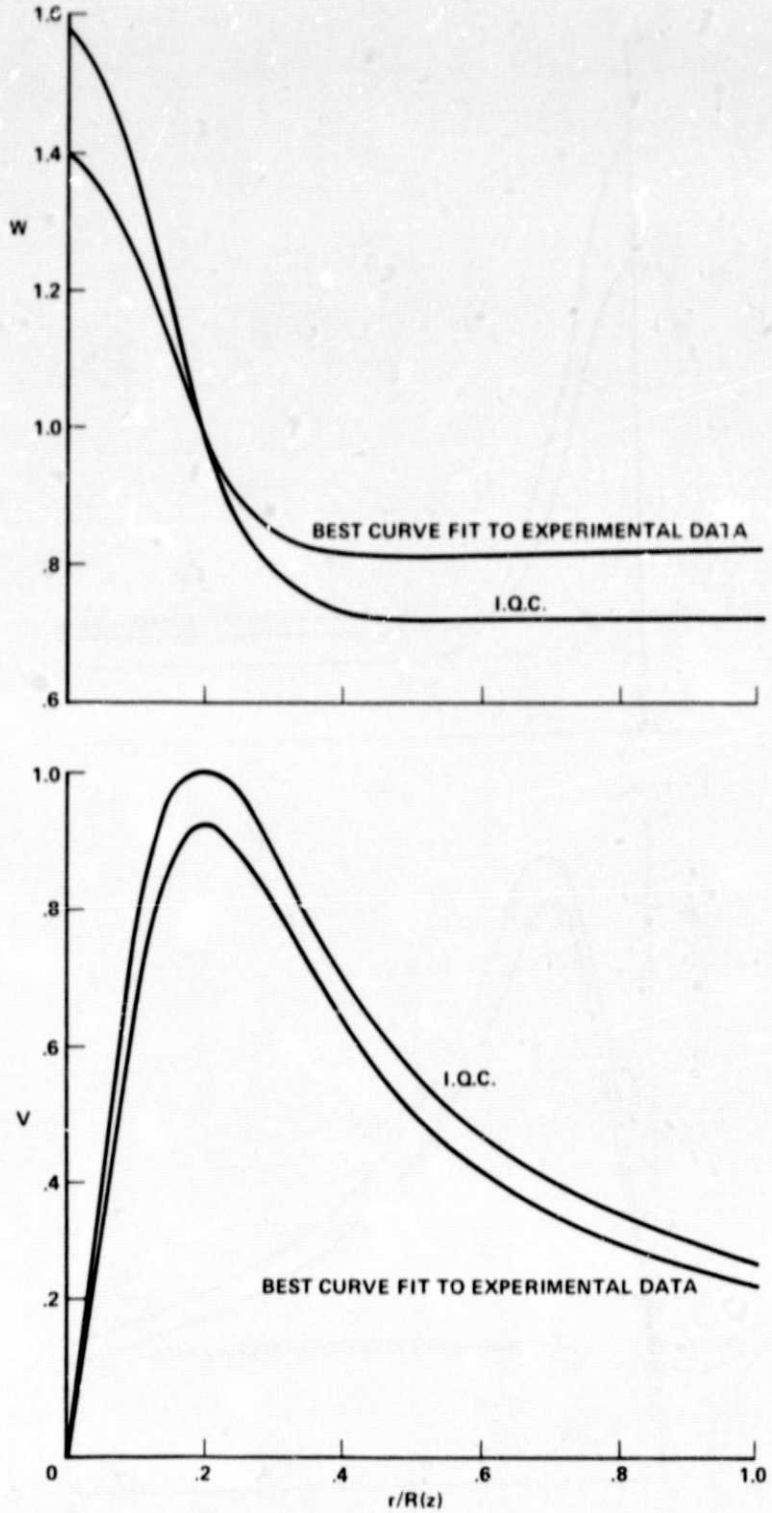

Figure 14.- Comparison of axial (W) and swirl (V) velocities between the best curve fit to experimental data and inviscid quasi-cylindrical solution (I.Q.C.) at axial station $z = 6.8$ for Re = 14100; $\Omega = 0.741$ at the inlet of the duct with shape; $R(z) = 1 + 0.025z$.

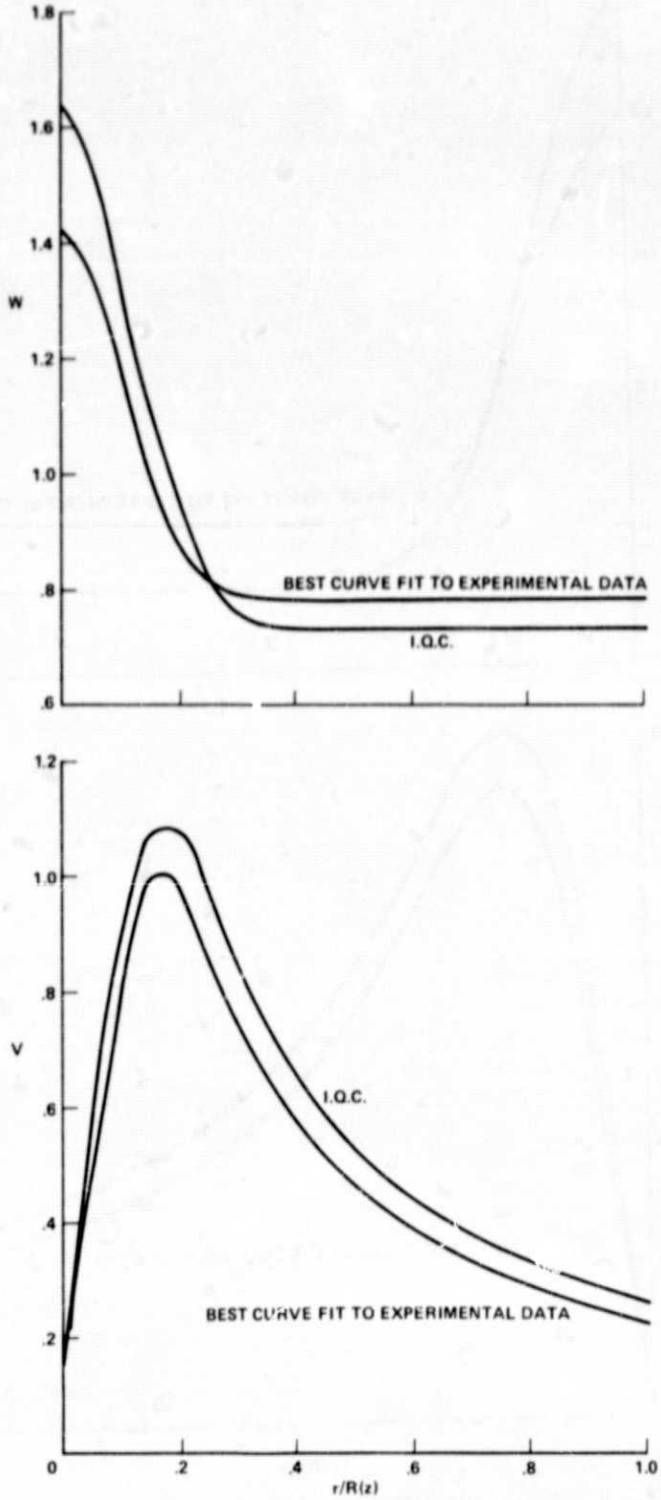

Figure 15.- Comparison of axial (W) and swirl (V) velocities between the best curve fit to experimental data and inviscid quasi-cylindrical solution (I. Q. C.) at axial station $z = 6.5$ for $Re = 20660$; $\Omega = 0.682$ at the inlet of the duct with shape; $R(z) = 1 + 0.025z$.

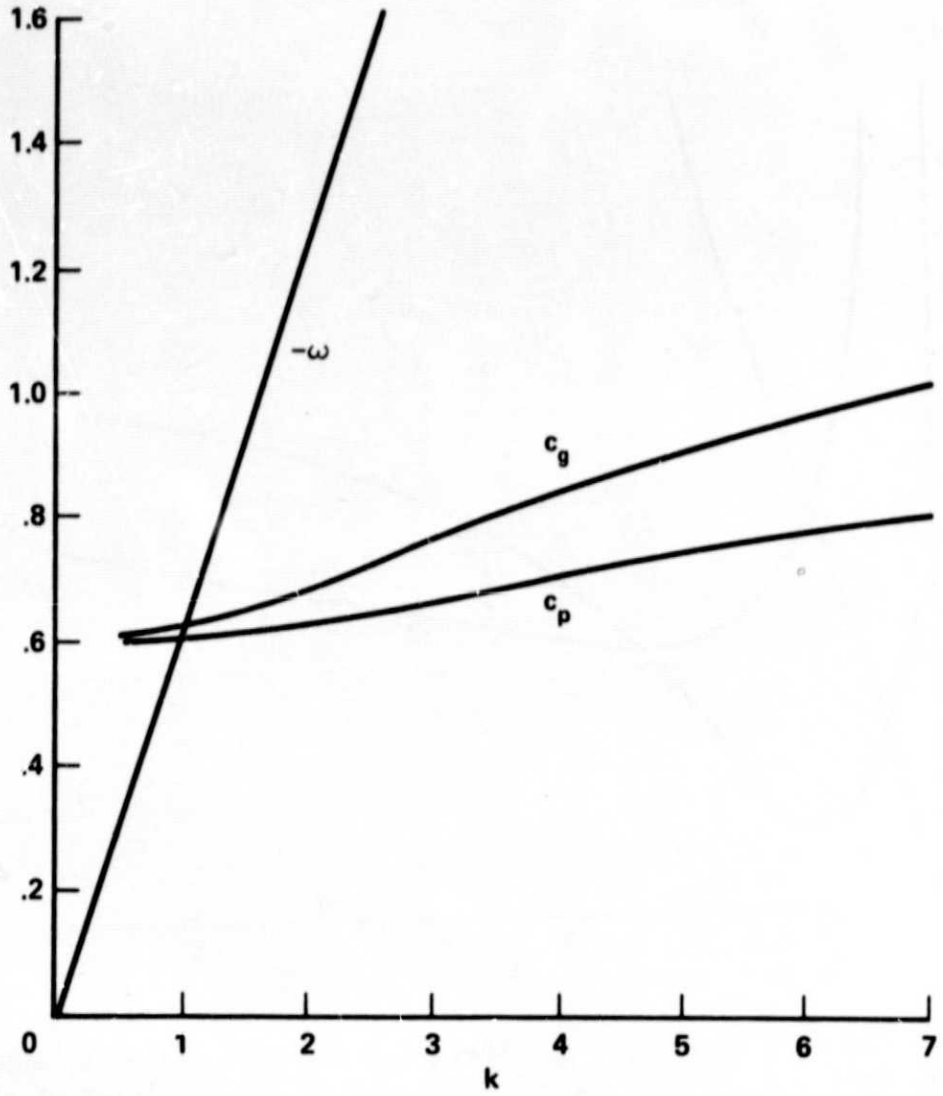

Figure 16.- Variation of frequency ω, phase velocity C_p and group velocity C_g vs wave number k of mode $n = 0$ for case (8) at the inlet of a divergent duct.

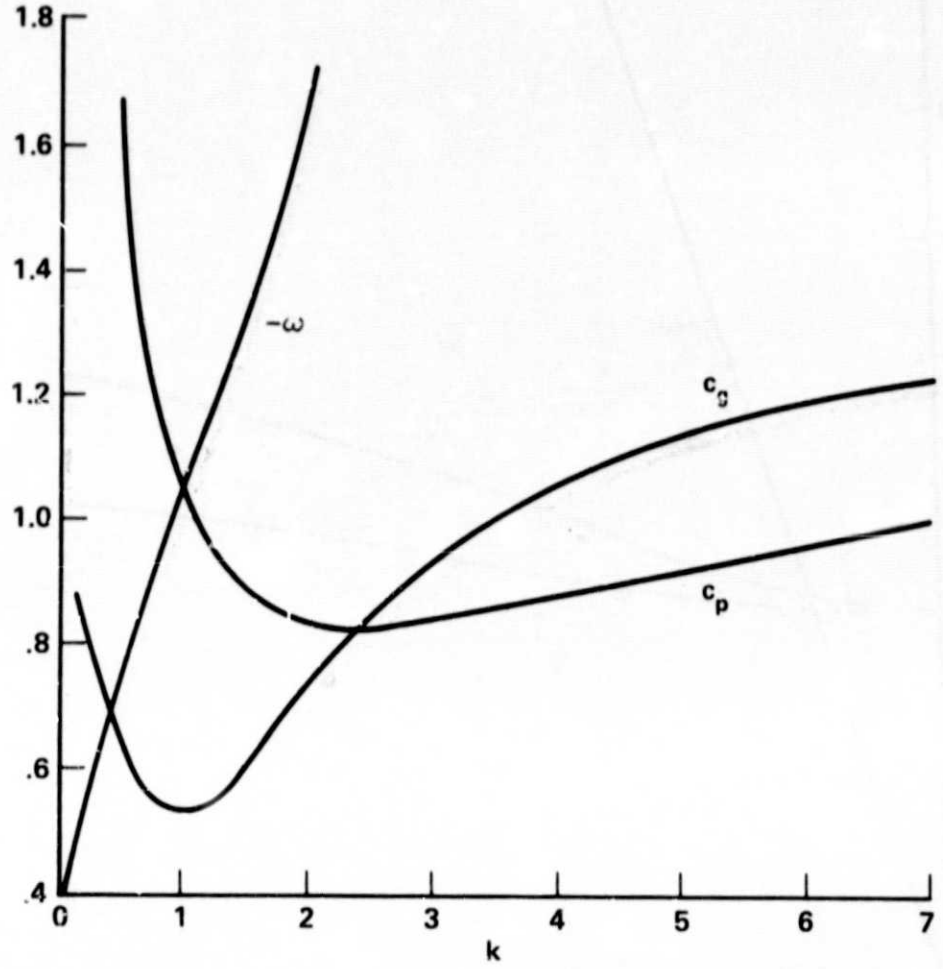

Figure 17.- Variation of frequency ω, phase velocity C_p and group velocity C_g vs wave number k of mode $n = 1$ for case (8) at the inlet of a divergent duct.

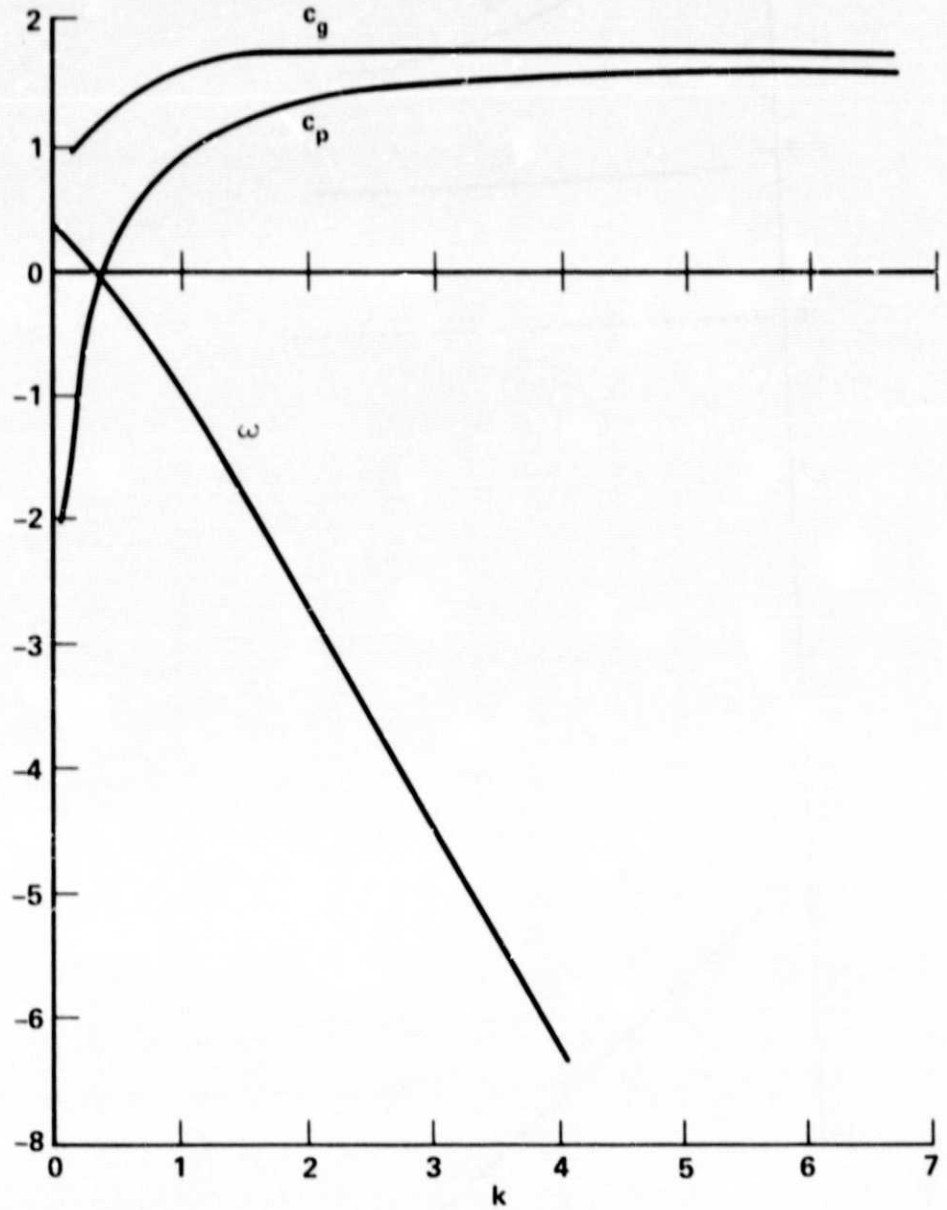

Figure 18.- Variation of frequency ω, phase velocity C_p and group velocity C_g vs wave number k of mode $n = -1$ for case (8) at the inlet of a divergent duct.

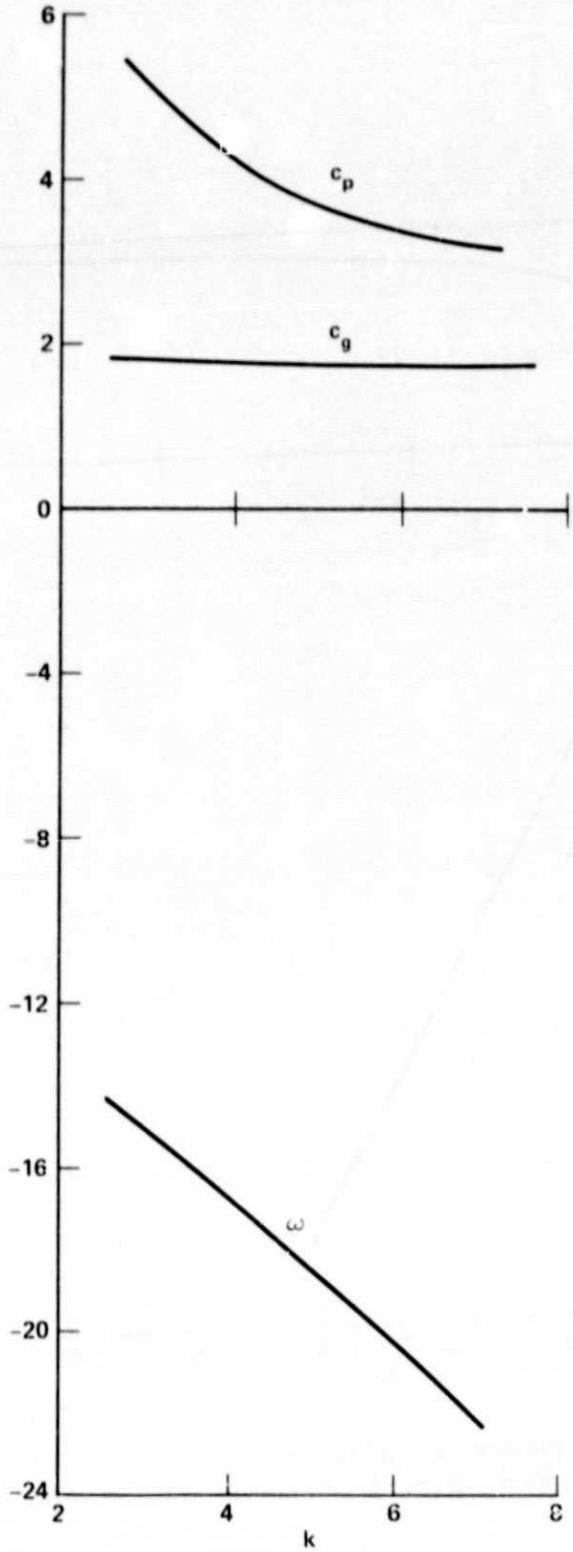

Figure 19.- Variation of frequency ω, phase velocity C_p and group velocity C_g vs wave number k of mode n = 2 for case (8) at the inlet of a divergent duct.

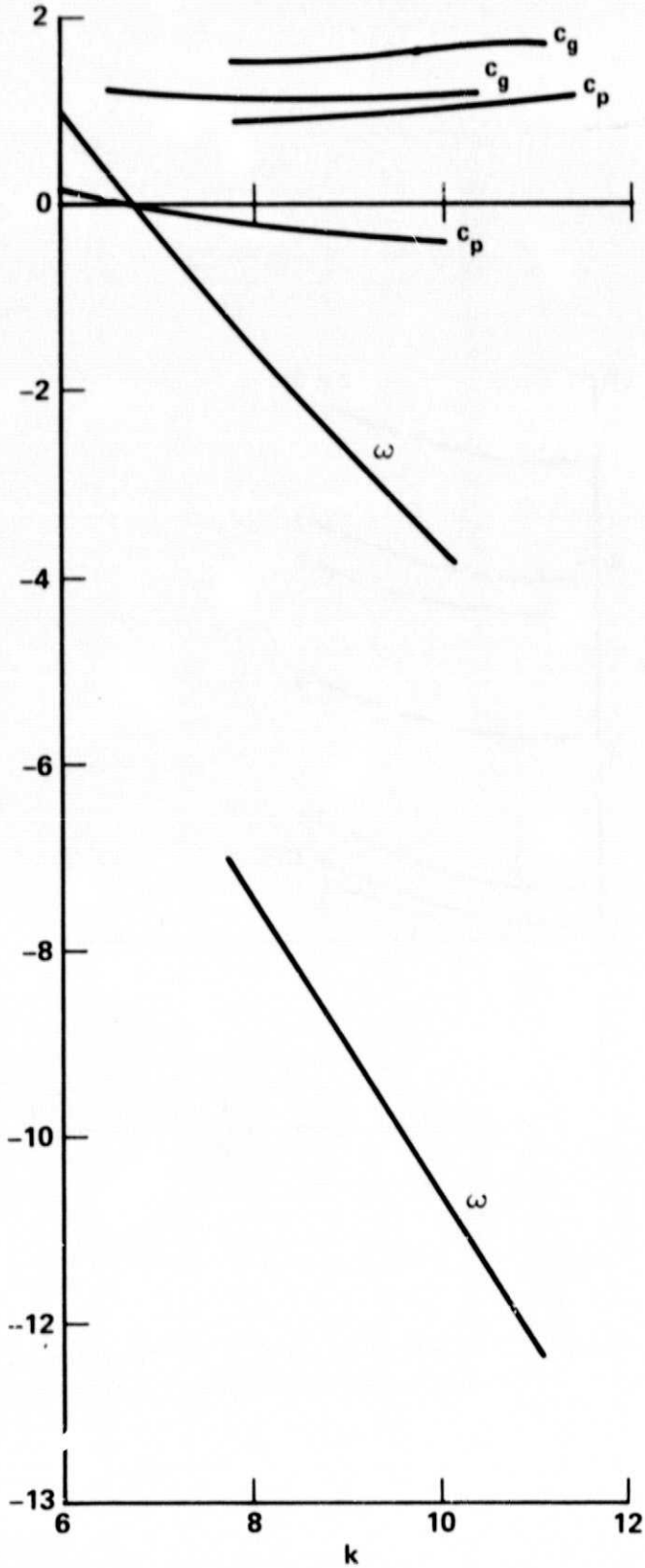

Figure 20.- Variation of frequency ω, phase velocity C_p and group velocity C_g vs wave number k of mode $n = -2$ for case (8) at the inlet of a divergent duct.

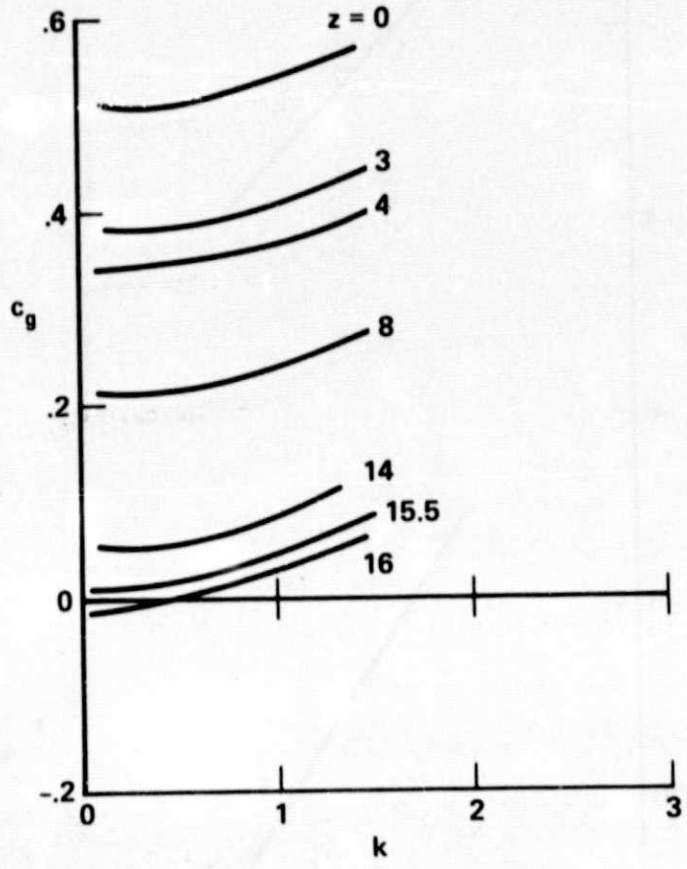

Figure 21.- The group velocities of mode n = 0 at various axial stations for case (4) in table 1. Inviscid quasi-cylindrical approximation fails near z = 16.5

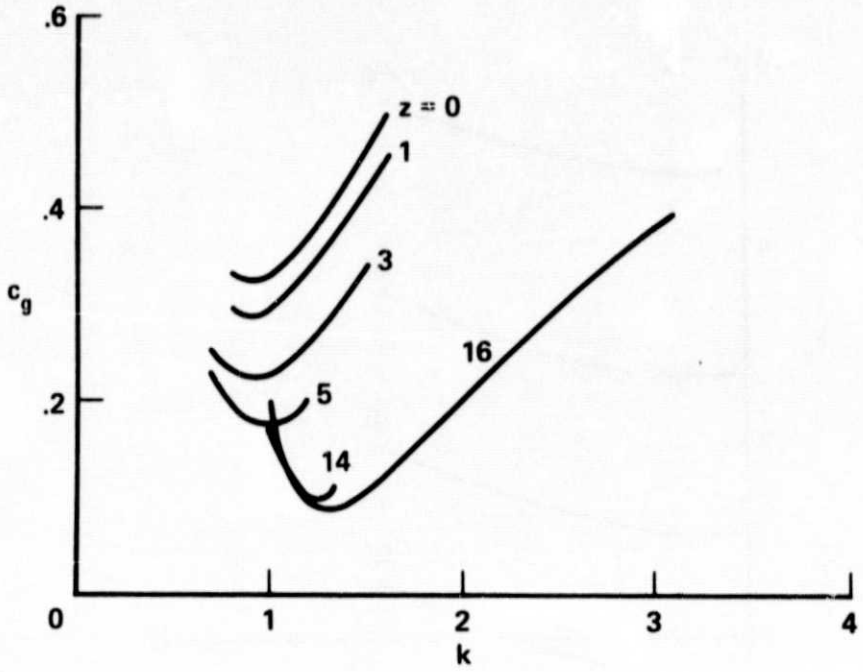

Figure 22.- The group velocities of mode n = 1 at various axial stations for case (4) in table 1.

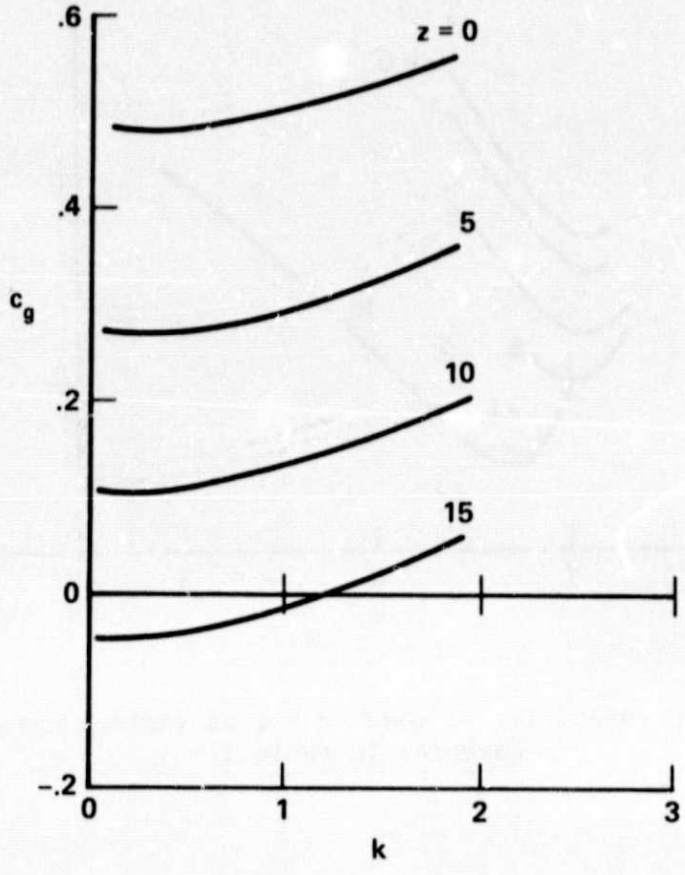

Figure 23.- The group velocities of mode n = 0 at various axial stations for case (1) in table 1. Inviscid quasi-cylindrical approximation fails near z = 15.5.

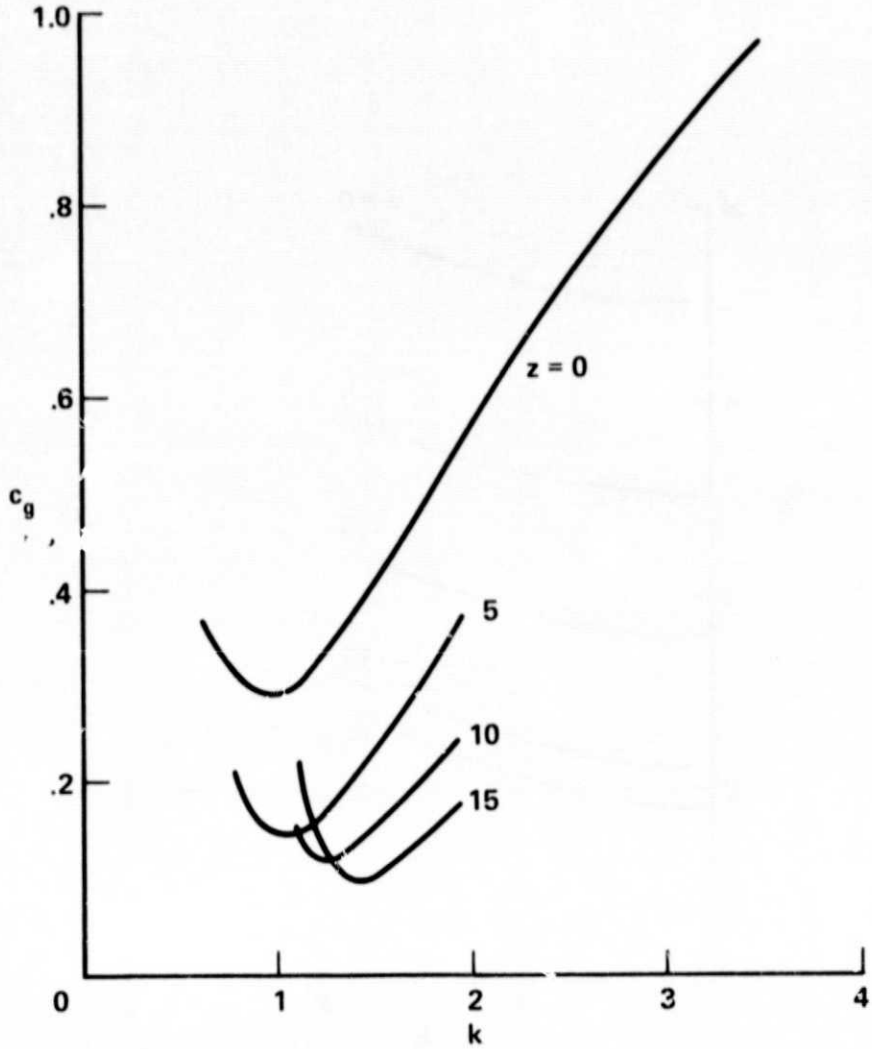

Figure 24.- The group velocities of mode n = 1 at various axial stations for case (1) in table 1.

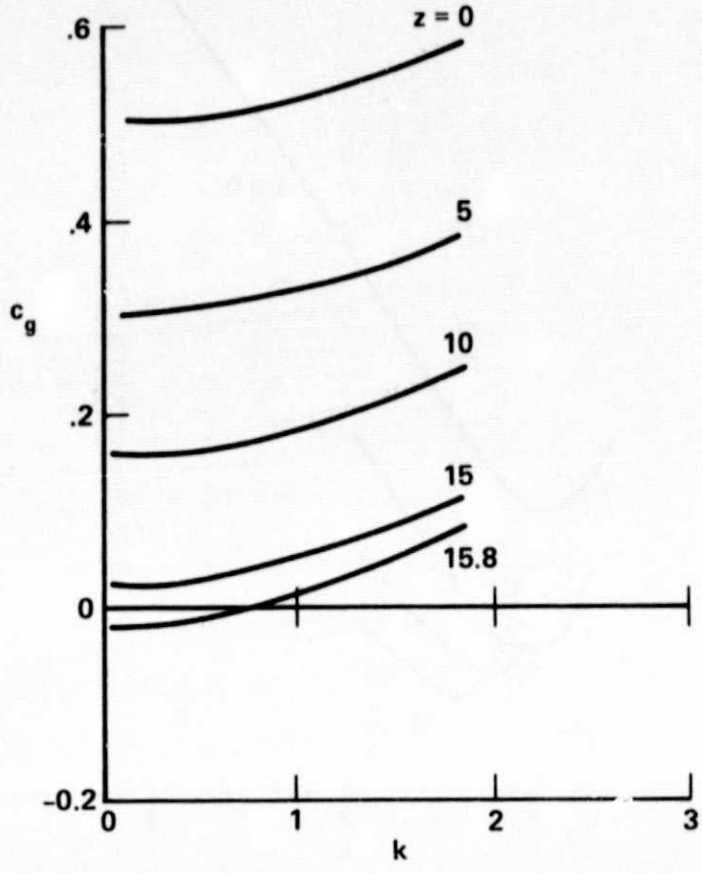

Figure 25.- The group velocities of mode n = 0 at various axial stations for case (2) in table 1. Inviscid quasi-cylindrical approximation fails near z = 16.2.

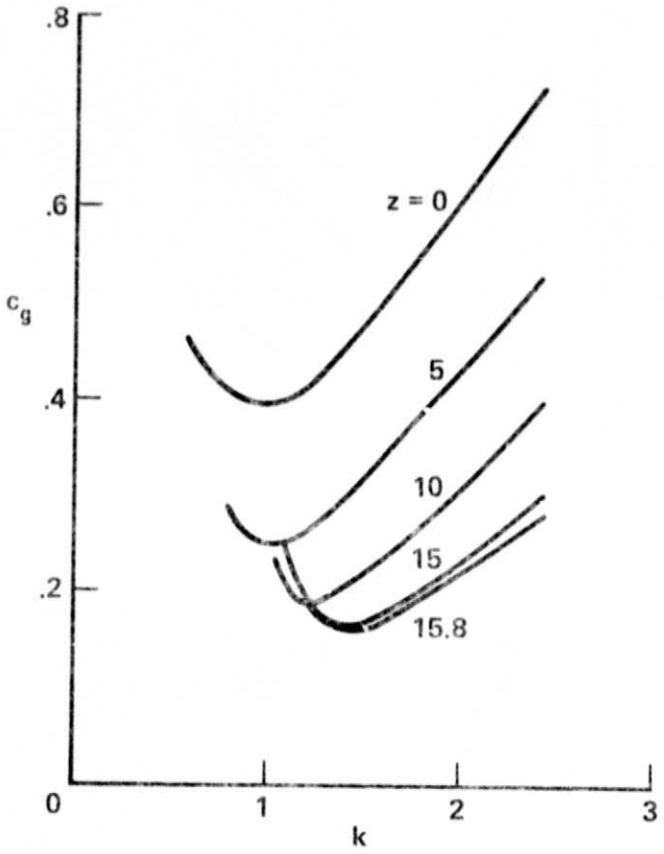

Figure 26.- The group velocities of mode n = 1 at various axial stations for case (2) in table 1.

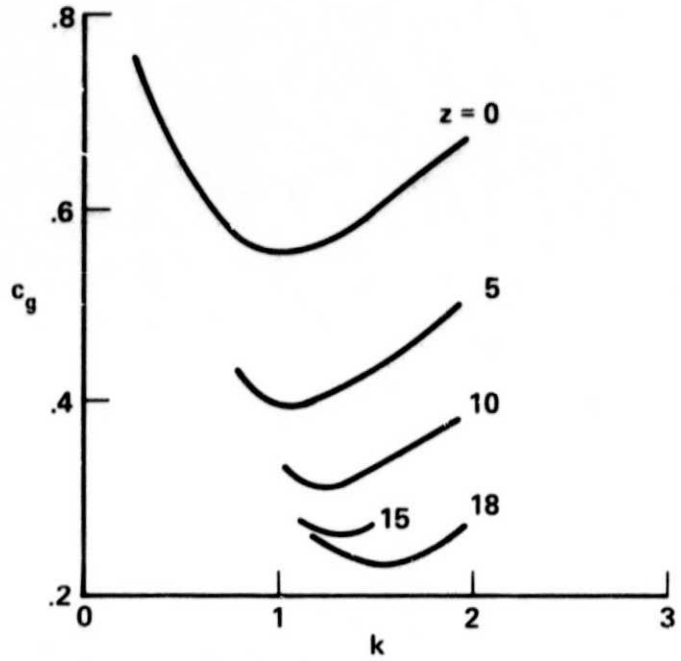

Figure 27.- The group velocities of mode n = 1 at various axial stations for case (3) in table 1. Inviscid quasi-cylindrical approximation fails near z = 18.5.